Evidence for a New Class of Defects in Highly n-Doped Si: Donor-Pair-Vacancy-Interstitial Complexes

P. M. Voyles,[1,*] D. J. Chadi,[2] P. H. Citrin,[1] D. A. Muller,[1] J. L. Grazul,[1] P. A. Northrup,[1] and H.-J. L. Gossmann[3]

[1]*Bell Laboratories, Lucent Technologies, Murray Hill, New Jersey 07974, USA*
[2]*NEC Laboratories America, Princeton, New Jersey 08540, USA*
[3]*Agere Systems, Berkeley Heights, New Jersey 07922, USA*

(Received 20 January 2003; published 19 September 2003)

Electron channeling experiments performed on individually scanned, single columns of atoms show that in highly n-type Si grown at low temperatures the primary electrically deactivating defect cannot belong to either the widely accepted class of donor-vacancy clusters or a recently proposed class of donor pairs. First-principles calculations suggest a new class of defects consisting of two dopant donor atoms near a displaced Si atom, which forms a vacancy-interstitial pair. These complexes are consistent with the present experimental results, the measured open volume of the defects, the observed electrical activity as a function of dopant concentration, and the enhanced diffusion of impurities in the presence of deactivated dopants.

DOI: 10.1103/PhysRevLett.91.125505 PACS numbers: 61.72.Ji, 61.72.Tt, 68.37.Lp

Silicon integrated circuit technology depends on the ability to introduce charge carriers locally into the host Si crystal by doping. Future generations of this technology will require carrier concentrations, n_e, $> 10^{20}$ cm^{-3} [1], but at the high dopant concentrations n_d needed for this not every dopant atom generates a carrier [2]. Determining why n_e saturates as a function of n_d is, therefore, clearly of significant practical importance. The formation of large dopant precipitates can be avoided with appropriate processing, so saturation of $n_e(n_d)$ must involve electrically deactivating defect clusters comprising only a few dopant atoms [2,3]. The structure and formation of these clusters depend on the atomic-level properties of impurities and point defects, making the clusters of fundamental scientific interest as well.

The most prevalent model for the structure of the deactivating defects in n-type Si consists of $i = 2$–4 Group V donor atoms, D, surrounding a vacancy, V, denoted D_iV. The neighboring vacancy renders both donor atoms threefold coordinated and electrically inactive. First-principles calculations have shown that forming D_3V or D_4V defects is exothermic [4], but forming DV or D_2V structures is endothermic [5]. A different class of defects, called a donor pair (DP) containing two donors and no vacancy, has recently been proposed [6]. The two lowest energy DP structures are DP(2) and DP(4), in which donor atoms occupy either second- or fourth-neighbor Si sites along a $\langle 110 \rangle$ direction. In each case, both donor atoms become threefold coordinated as a result of a Si lattice reconstruction and the recapture of two electrons from the Fermi sea, which pins the Fermi level [6]. Schematic diagrams for D_2V and DP(2) defects with $D =$ Sb are shown in Fig. 1.

Single dopant atoms of Sb embedded within a bulk Si crystal can be imaged using annular dark-field "Z-contrast" scanning transmission electron microscopy (ADF-STEM) [7]. These images show that, in highly Sb-doped Si grown at low temperatures, the primary deactivating defect contains only two Sb atoms [7], which rules out the energetically favorable Sb_3V and Sb_4V models, leaving only Sb_2V, DP(2), and DP(4) as viable candidates. Which type of defect dominates is crucial to understanding the saturation of $n_e(n_d)$: Sb_2V depends on a preexisting population of vacancies [5,8], while DP(2) and DP(4) do not [6].

Here, using additional STEM measurements, x-ray absorption (XAS) data, and first-principles calculations, we show that neither Sb_2V nor DP(2) defects are important in highly Sb-doped Si. We propose instead a new class of defect, the donor-pair-vacancy-interstitial complex, which is consistent with all these structural data, has a reasonable formation energy, and accounts for a wide range of other experimental results.

STEM measurements are sensitive to Δr_{Sb}, the distance of the Sb atoms from their substitutional sites. As

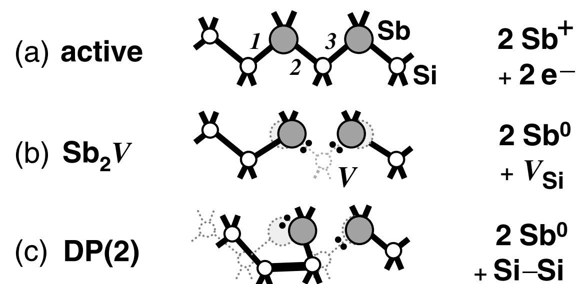

FIG. 1. Schematic diagram for forming electrically deactivating defects from (a) two active Sb atoms in Si. (b) An Sb_2V is formed by breaking bonds 2 and 3 and creating a Si vacancy. (c) A DP(2) is formed by breaking bonds 1 and 3 and forming a new Si-Si bond, shown bold. The resulting displacements of the Sb and Si atoms are indicated.

 © 2003 The American Physical Society

shown schematically in Fig. 1, Δr_{Sb} is much larger in DP(2) than in Sb_2V. Below, we describe a new approach for using STEM to measure Δr_{Sb}, then compare these measurements to first-principles calculations of the defect structures, and finally present the new donor-pair-vacancy-interstitial defect.

An ADF-STEM image is formed by raster scanning a small electron probe and collecting the high-angle scattering. With a sufficiently small probe, we could in principle image Δr directly, but in practice this is currently not possible. We can, however, take advantage of the fact that a probe incident on a crystal oriented on a high-symmetry zone axis channels very strongly down the nearest columns of atoms [9]. Since the signal from a heavy impurity atom is proportional to the local probe intensity at the impurity [10,11], channeling will enhance the image intensity of an on-column impurity. The image intensity will therefore decrease as Δr increases.

Measurements based on absolute intensities in electron micrographs are generally fraught with difficulties. In our case, the image intensity of an impurity depends not only on its Δr but on its depth in the sample and on the surface conditions. We use very thin, clean, and smooth samples to minimize these effects [7], but comparing intensities in two images allows us to remove them almost entirely. By tuning the inner angle of the annular detector, we can adjust the relative contributions to the image of the Rutherford scattering from the impurity atom and the coherent diffraction from the Si lattice. We therefore acquire two images using the detector arrangement shown in the top left of Fig. 2: a high-angle (HA) detector spanning 50–250 mrad scattering angle, and a low-angle (LA) detector spanning 14–50 mrad. Both images are collected simultaneously from the same probe scan, so they are guaranteed to be in exact registration.

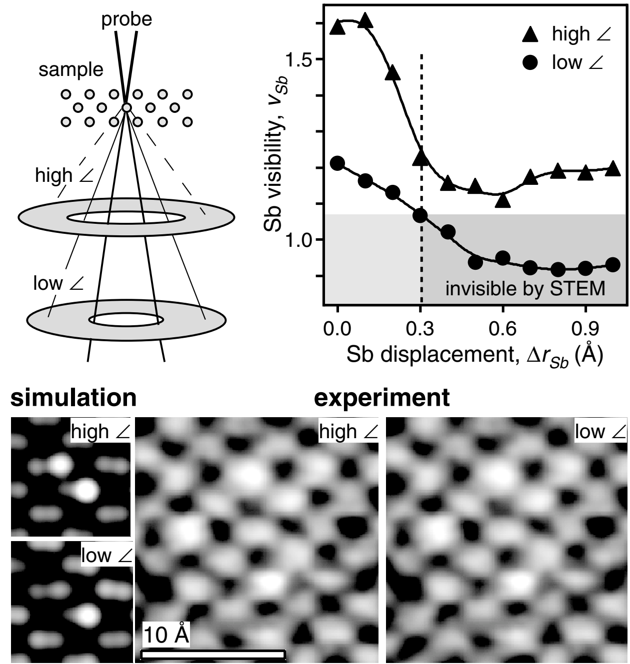

FIG. 2. (top left) STEM detector configuration: The dashed line is high-angle scattering caught on the upper detector, the light line is low-angle scattering caught on the lower detector, and the heavy line is unscattered electrons, which are not detected. (top right) Simulated visibility of a single Sb atom in 40 Å of Si as a function of Δr_{Sb}, the projected off-column displacement of the Sb atom. The Sb atom is not visible in the low-angle image for $\Delta r_{\mathrm{Sb}} > 0.3$ Å. (bottom left) Simulated images of a DP(2) defect. The off-column Sb atom is visible in the high-angle image, but not in the low-angle. (bottom right) Experimental images. The brightest spots are atomic columns containing at least one Sb atom. These features appear on the same columns in both high- and low-angle images, indicating experimentally that for these Sb atoms $\Delta r_{\mathrm{Sb}} <$ 0.3 Å. Images have been smoothed and had pixels added by interpolation.

On the top right, Fig. 2 shows the visibility, $v_{\mathrm{Sb}} = I_{\mathrm{Sb}}/I_{\mathrm{Si}}$, simulated with a plane-wave multislice algorithm of a single Sb atom in 40 Å of Si as a function of Δr_{Sb} for our detectors. We consider an impurity "visible" if its v_{Sb} exceeds the $\sim$5% noise level in our images. The Sb atom is always visible in the HA image: $v_{\mathrm{Sb}}(\Delta r_{\mathrm{Sb}})$ decreases rapidly up to 0.4 Å, after which it levels off and starts increasing for $\Delta r_{\mathrm{Sb}} \geq 0.7$ Å because the off-column Sb atom begins to be resolved. (We are unlikely to observe this experimentally due to noise in the STEM scan system.) In the LA image, the Sb is visible for $\Delta r_{\mathrm{Sb}} < 0.3$ Å, but invisible for $\Delta r_{\mathrm{Sb}} > 0.3$ Å because the Si lattice intensity is greater than in the HA image. Simulations tend to overestimate the contrast in electron micrographs [12], so the cutoff may be somewhat less than 0.3 Å, but it will not be larger.

We can use the HA image to locate essentially all the Sb atoms in the sample [7], then determine whether their Δr_{Sb} is greater or less than 0.3 Å by looking for an Sb in the same place in the LA image: If an Sb is not visible, then its $\Delta r > 0.3$ Å. This effect is shown in simulated images of a DP(2) defect in the lower left of Fig. 2. Both Sb atoms are visible in the HA image, but the Sb with a large Δr_{Sb} (see Fig. 1) disappears in the LA image. The Δr cutoff can be changed by tuning the inner angle of the LA detector, but (see below) 0.3 Å is useful for Sb.

Note that while the average Δr of impurities in a crystal can be measured using x-ray standing waves [13] or Rutherford backscattering and ion channeling [14], our STEM-based approach has the ability to measure Δr one impurity atom at a time. This is particularly important for studying defects because we can focus on the Δr of only those impurities whose lattice positions are consistent with a pair defect.

The electronic and structural properties of various defects were examined via *ab initio* pseudopotential total-energy calculations as in Ref. [6]. We used a 64-atom cubic supercell, a Brillouin-zone sampling of average energies at the zone center and boundaries, and an energy cutoff of

TABLE I. ⟨110⟩-projected off-column distances and formation energies for various pair defect models (see text).

Model	Δr_{Sb_2} (Å)	Δr_{Sb_3} (Å)	ΔE_0 (eV)
Sb_2V	0.37	0.36	0.87
DP(2)	1.10	0.64	0.63
DP(4)	0.30	0.29	0.30
DP(2)V-I	0.28	0.15	0.45
DP(4)V-I	0.33	0.19	0.30

16 Ry energy for the plane-wave expansion. Table I gives selected off-column displacements for the calculated structures. There are three unique ⟨110⟩ orientations. In orientation 1, the two Sb atoms occupy the same column in projection and are not resolved. Δr_{Sb_2} and Δr_{Sb_3} in Table I are the larger of the two Sb displacements in orientations 2 and 3. The other Sb atom in each case has $\Delta r_{Sb} < 0.2$ Å, except for Sb_2V in orientation 3, where both Sb atoms have $\Delta r_{Sb} = 0.36$ Å. Table I also shows formation energies, ΔE_0. The formation energy for a pair defect relative to the energy of two Sb^+ ions is given by $\Delta E = \Delta E_0 - 2E_F$, where E_F is measured from the conduction band edge.

STEM measurements were made on Sb-doped Si samples prepared by low-temperature molecular beam epitaxy (LT-MBE) [6,7]. Images were acquired in a JEOL-2010F STEM ($C_s = 1.0$ mm, 200 kV, 10 mrad convergence, and 450 Å defocus; STEM simulations used these parameters). Three areas of the sample were investigated, with thicknesses of 32, 30, and 23 Å, all ± 2 Å. Procedures for TEM sample thinning, thickness measurement, and image processing to identify Sb-containing columns have been described elsewhere [7,15]. Results are reported for an intensity threshold in units of the background standard deviation of 1.2σ per pixel over five pixels, which puts the false positive rate from random intensity variations at the 6σ level per atom.

In the sample studied, $n_d = 9.35 \times 10^{20}$ cm^{-3}, measured by Rutherford backscattering, and $n_e = 6.5 \times 10^{20}$ cm^{-3}, measured by Hall effect; 30% of the Sb atoms are therefore electrically inactive. For DP(2), Δr_{Sb_2} and $\Delta r_{Sb_3} > 0.3$ Å, so 10% of the Sb atoms that appear in the HA image should disappear in the LA image. For Sb_2V, both Sb atoms in orientation 3 have $\Delta r_{Sb_3} > 0.3$ Å, so 15% of the Sb atoms should disappear.

This effect is not observed. Portions of one of the experimental HA and LA images are shown in Fig. 2. The brightest atomic columns in the HA image are Sb-containing columns, most of which contain only one Sb [7]. These bright columns appear in the same positions in the LA image, which is typical. Of the 438 Sb atoms detected in the full field HA image of the 32-Å thick sample, only 13, or 3.0% ± 0.8%, were not detected in the corresponding LA image. A similar fraction was found in the LA image and not the HA; these are false positives due to sample roughness and a submonolayer oxide coverage. In the two other images, 4% ± 1% of 381 and 4% ± 1% of 369 Sb atoms disappear.

If the sample contained a mixture of several defects, such as DP(2) and DP(4), the disappearing fraction of Sb atom images would be proportionally smaller. However, those Sb atom images that did disappear would still tend to be in lattice positions associated with a pair defect. We observe no statistically significant trend for the disappearing Sb atom images to be in pair defect lattice sites, and attribute all the disappearances to be false positives in the HA image.

We therefore conclude that the primary deactivating pair defect in this sample is neither DP(2) nor Sb_2V, and must have a smaller Δr_{Sb} than either of them. Revisiting earlier XAS data [6] shows that it is also inconsistent with DP(2). Previous simulations had assumed a symmetric Δr_{Sb} for the two Sb atoms in the DP defects, which is correct for DP(4) but not for DP(2). Simulations for the actual asymmetric configuration are inconsistent with the data. Moreover, the improved 16 Ry energy cutoff in our current calculations puts the DP(2) formation energy at 0.63 eV, not 0.26 eV as previously calculated [6]. [Only a single zone sampling had been used for the DP(2) defect, giving incomplete convergence with a 12 Ry cutoff energy. Convergence of our new calculations for DP(2) was confirmed by testing energy levels and structural parameters with a cutoff of 25 Ry.] The formation energy of Sb_2V is also large, at 0.87 eV. These defects might still be formed by vacancy-assisted diffusion [5], but that assumes a preexisting vacancy population, and a deliberate excess of vacancies has been found to have no effect on the kinetics of dopant deactivation [16]. Vacancies are created by high-temperature sample preparation and by dopant-ion implantation, but vacancy formation is minimized in the LT-MBE sample studied here [17]. Thus, while Sb_2V defects may exist in, e.g., implanted samples, they do not represent an intrinsic limit on $n_e(n_d)$.

DP(4) is then the only remaining defect. It has been shown that, assuming random substitution of Sb in the Si lattice (which is confirmed by ADF-STEM images [7,15]), a model with 28 deactivating sites gives a good fit to the experimental $n_e(n_d)$ [6]. A model with only DP(4) defects and Sb dimers has only 16 such sites, which gives a very poor fit, ruling out DP(4) defects alone.

Accordingly, we propose a new class of donor impurity defects in Si consisting of a pair of donor atoms and a displaced Si atom that forms a Si vacancy, V, and a Si interstitial, I. This defect, which is suggestive of a hybrid between a donor-pair and a Frenkel-pair defect, is denoted DP(i)V-I. The donor atoms occupy the same lattice positions as in the corresponding DP(i) defect [6]. Figure 3 is a schematic diagram of a donor-pair-vacancy-interstitial defect with $i = 2$. The Sb atom near the vacancy is threefold coordinated and neutral. The

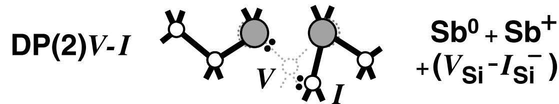

FIG. 3. Schematic of the DP(2)V-I deactivating defect. Referring to Fig. 1, DP(2)V-I is formed by breaking bond 2 and forming a Si vacancy-interstitial pair. The resulting Sb-atom displacements are smaller than in either Sb_2V or DP(2).

other Sb is fourfold coordinated and positively charged, but the nearby, negatively charged interstitial Si renders the entire defect neutral.

Like the DP(i) defects, the DP(i)V-I defects are Fermi-level pinning. At saturated n_e, E_F lies $\simeq 0.2$ eV above the conduction band minimum [6], so ΔE_0 for these pair defects must be less than 0.2 eV per Sb. DP(2)V-I and DP(4)V-I meet this criterion within kT at room temperature. Other DP(i)V-I defects were tested, but all had unrealistic ΔE_0 values.

The Sb atoms in these defects remain closer to their substitutional sites than in Sb_2V or DP(2) (see Fig. 3 and Table I). Most of the structural distortion associated with DP(i)V-I is concentrated in the V-I pair, whereas DP(4) involves several large Si displacements and the formation of a three-membered Si ring. DP(2)V-I has the smallest Δr_{Sb}, consistent with our STEM measurements. DP(4)V-I might lead to a few HA/LA disappearances, since Δr_{Sb_2} is slightly larger than 0.3 Å, but it is also consistent with the data. Simulated XAS spectra from DP(2)V-I and DP(4)V-I are in excellent agreement with experiment. If we consider Sb dimers, DP(2)V-I, DP(4)V-I, and DP(4) defects, we again have 28 sites around a donor where deactivation can occur, which fits the $n_e(n_d)$ data. This group of defects also preserves the geometric frustration explanation of enhanced n_e in dopant δ layers [18]. None of these defects requires a preexisting vacancy, so they represent an intrinsic limit on n_e.

The Fermi-level pinning nature of these defects reconciles ADF-STEM images of the Sb-pair populations in potential DP(2)/DP(2)V-I and DP(4)/DP(4)V-I sites; if all the Sb atoms were electrically inactive, the images would predict 50% electrical inactivity rather than the observed 30% [7]. However, because E_f has already been pinned by some fraction of existing defects, not all of those Sb atoms have sufficient energy to form defect structures and become deactivated.

DP(i)V-I defects also explain positron annihilation spectroscopy (PAS) measurements and dopant-enhanced diffusion. PAS shows that defects in highly n-type Si involve significant open volume, which had been attributed to a V [19]. While the DP(i) defects have open volume created by bond reconstruction, it is too small to explain recent PAS data [20]. The DP(2)V-I defects are calculated to have open volume even greater than that of Sb_2V. Recent PAS measurements and analysis of the same LT-MBE grown, Sb-doped sample studied here are consistent with a combination of DP(2)V-I and DP(4)V-I or Sb_2V and SbV [21]. Similarly, enhanced impurity diffusion in highly n-type Si had been explained by the presence of V and I point defects associated with the deactivating defect [22,23]. DP(i)V-I generates these very defects. At high temperatures, the V and the I become mobile, assist in diffusion of other species, and leave behind D_nV structures that could grow as previously described [5,8].

In summary, we have shown that neither donor-pair nor vacancy-centered donor-cluster defects can account for the observed electrical deactivation in highly n-doped Si. A new class of Fermi-level pinning defects is proposed containing both a donor-atom pair and a Si vacancy-interstitial pair. The new defect structures are consistent with STEM and XAS data, with electrical carrier behavior versus dopant concentration, and with measurements of enhanced diffusion and open volume.

*Current address: University of Wisconsin, Madison, WI 53706, USA.
Electronic address: voyles@engr.wisc.edu

[1] H.-J. Gossmann *et al.*, Mater. Res. Soc. Symp. Proc. **610**, B1.2.1 (2000).
[2] J. S. Williams and K. T. Short, J. Appl. Phys. **53**, 8663 (1982).
[3] A. Nylandsted Larsen *et al.*, J. Appl. Phys. **59**, 1908 (1986).
[4] K. C. Pandey *et al.*, Phys. Rev. Lett. **61**, 1282 (1988).
[5] M. Ramamoorthy and S. T. Pantelides, Phys. Rev. Lett. **76**, 4853 (1996).
[6] D. J. Chadi *et al.*, Phys. Rev. Lett. **79**, 4834 (1997).
[7] P. M. Voyles *et al.*, Nature (London) **416**, 826 (2002).
[8] and , Appl. Phys. Lett. **42**, 1043 (1983); J. Appl. Phys. **66**, 970 (1989).
[9] J. Fertig and H. Rose, Optik **59**, 407 (1981).
[10] R. R. Vanfleet *et al.*, in *Characterization and Metrology for ULSI Technology: 1998 International Conference*, edited by D. G. Seiler *et al.* (American Institute of Physics, Woodbury, NY, 1998), pp. 901–905.
[11] P. M. Voyles *et al.*, Microsc. Microanal. (to be published).
[12] C. B. Boothroyd, J. Microsc. **190**, 99 (1998).
[13] A. Herrera-Gómez *et al.*, J. Appl. Phys. **85**, 1429 (1999).
[14] C. Brizard *et al.*, J. Appl. Phys. **75**, 126 (1994).
[15] P. M. Voyles *et al.*, Ultramicroscopy (to be published).
[16] S. Solmi *et al.*, Appl. Phys. Lett. **80**, 4774 (2002).
[17] H.-J. Gossmann *et al.*, J. Appl. Phys. **73**, 8237 (1993).
[18] P. H. Citrin *et al.*, Phys. Rev. Lett. **83**, 3234 (1999).
[19] D. W. Lawther *et al.*, Appl. Phys. Lett. **67**, 3575 (1995).
[20] K. Saarinen *et al.*, Phys. Rev. Lett. **82**, 1883 (1999).
[21] M. Rummukainen *et al.* (to be published).
[22] R. B. Fair and G. R. Weber, J. Appl. Phys. **44**, 273 (1973).
[23] J. Fage-Pederson *et al.*, J. Appl. Phys. **88**, 3254 (2000).